NRIAG Journal of Astronomy and Geophysics (2013) 2, 146–165

National Research Institute of Astronomy and Geophysics

NRIAG Journal of Astronomy and Geophysics

www.elsevier.com/locate/nrjag

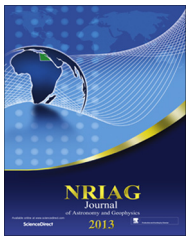

Estimating the near-surface site response to mitigate earthquake disasters at the October 6th city, Egypt, using HVSR and seismic techniques

Adel M.E. Mohamed [a,b,*], H.E. Abdel Hafiez [a], M.A. Taha [a]

[a] *National Research Institute of Astronomy and Geophysics (NRIAG), Egypt*
[b] *Earthquake Monitoring Center (EMC), Sultan Qaboos University (SQU), Sultanate of Oman*

Received 30 October 2012; accepted 21 May 2013
Available online 1 July 2013

KEYWORDS

HVSR;
Seismic refraction;
MASW;
Natural period;
Pulse-width;
Site response

Abstract The damage caused by earthquake occurrences in different localities necessitates the evaluation of the subsurface structure. A priori estimation of the site effects became a major challenge for an efficient mitigation of the seismic risk. In the case of moderate to large earthquakes, at some distances from large events, severe damage often occurred at zones of unfavorable geotechnical conditions that give rise to significant site effects. The damage distribution in the near-source area is also significantly affected by fault geometry and rupture history. The microtremor (background noises) and shallow seismic surveys (through both the seismic refraction and Multi-channel Analysis of Surface Waves (MASW)) were carried out in a specific area (The club of October 6 city and its adjacent space area). The natural periods derived from the HVSR (Horizontal to Vertical Spectral Ratio) analysis vary from 0.37 to 0.56 s. The shallow seismic refraction data, which were conducted at the area, are used to determine the attenuation of P-waves (Q_p) in different layers, using the pulse-width technique. The evaluation of the site response at the studied area yields amplification factor of the ground motion, ranging between 2.4 and 4.4.

1. Introduction

The damage to human infra-structures and the disturbances of the local life affairs represent an inestimable cost for the national and local authorities, usually requiring international cooperation. Most of the crowded cities and high populated areas (as Cairo City) are located on soft sediments (valleys, estuaries, recent deposits, etc.), the soil structure of which is prone to amplify seismic waves (Murphy and Shah 1988; Bard 1994). This phenomenon is usually called site effect or site amplification, since the amplitude of the motion highly

* Corresponding author. Tel.: +20 2 25560645.
E-mail address: Geotec_04@yahoo.com (A.M.E. Mohamed).
Peer review under responsibility of National Research Institute of Astronomy and Geophysics.

2090-9977 © 2013 Production and hosting by Elsevier B.V. on behalf of National Research Institute of Astronomy and Geophysics.
http://dx.doi.org/10.1016/j.nrjag.2013.06.018

depends upon the local properties of the soil. The site response (transfer function) is evaluated through the geotechnical parameters (layer thicknesses, densities, boreholes. The P-wave velocities are obtained from the shallow seismic refraction survey (Mohamed, 2003, 2009; Mohamed et al., 2008) and the S-wave velocities are deduced from the Multi-channel Analysis of Surface Waves (MASW) survey.

The investments necessary for conventional techniques, i.e. boreholes, are prohibitive for developing countries and for regions of a moderate seismic activity. One of the most important and commonly encountered problems in geotechnical earthquake engineering is the evaluation of ground response. Moreover, it is commonly known that, during earthquakes, the damage to structures is reasonably associated with the underlying subsoil conditions. So, the dynamic properties of the underlying soils are greatly reflected by the characteristics of earthquake ground motions at the ground surface (i.e., ground response). It has, also, been demonstrated that, the geographic distribution of the ground shaking-related damage and its intensity are strongly dependent on the local lithological and physical properties (e.g., silt and clay content, as well as void ratio) and conditions (depth-to-water table and basement relief) of the near-surface sediments (Minakami and Sakuma, 1948; Kanai, 1952; Ooba, 1957; Mueller et al., 1982).

Consequently, understanding of the soil effect on the propagated seismic wave became an urgent need, in order to map areas, where amplification is likely and conveying this information to emergency managers and community officials. Moreover, it can be used in land-use planning, reducing business vulnerability, retrofitting building, producing guidelines for new constructions and assisting in infrastructure upgrading. Therefore, over the years, a great effort has been done in the level of theory (e.g., Ohsaki, 1981; Kramer, 1996) and level of application (e.g., Faeh et al., 1993, 1994; Panza et al., 1996).

The Horizontal to Vertical Spectral Ratio (HVSR) technique (Nakamura, 1989) for the noise survey (microtremor) is now widely used to estimate the site effect parameters (fundamental frequency and mostly the associated soil amplification), in which many surveys using this technique have provided convincing results (see Bard, 1999, for a review). However, a general agreement of a methodology for the data acquisition, data processing and results interpretation has yet to be found. The current study considers the study of the reliability of a low-cost method, based on the measurement of ambient vibrations. The focus was put on the so-called HVSR (Horizontal-to-Vertical Spectral Ratio), which became widely used after the work of Nakamura (1989).

The objective of this research is to estimate the fundamental frequencies (natural periods) at the 6th of October club area and its extension (Fig. 1), where a part of the area is occupied by a swimming pool, playground and some gardens. The rest of the area is still empty. The obtained parameters; such as the fundamental frequency, will be integrated with the previous calculated geotechnical information (Mohamed et al., 2012), in order to evaluate the site response and the seismic hazard, which will be valuable for designing and constructing the space area.

2. Geologic Setting

The surface geology in and around the studied area (Fig. 2) reveals that, the oldest rocks are the Upper Cretaceous rocks, represented by Bahariya Formation, Abu Roash Formation and Khoman Formation. Then, the Tertiary rocks are represented by the Upper Eocene (Maadi Formation), the Oligocene rocks (Gebel Qatrani Formation and the Basalt flows), the Lower Miocene (Gebel Khashab Formation), the Pliocene (undifferentiated Pliocene deposits) and the Quaternary deposits (Nile sediments). All the investigated sites are occupied by Gebel Qatrani Formation. This formation is represented by a sequence of continental to littoral marine alternating clastics, burrowed siltstone, and reddish claystone (as derived from the surface geological map and the drilled boreholes). In general, the surface sediments in the studied area are loose to very loose

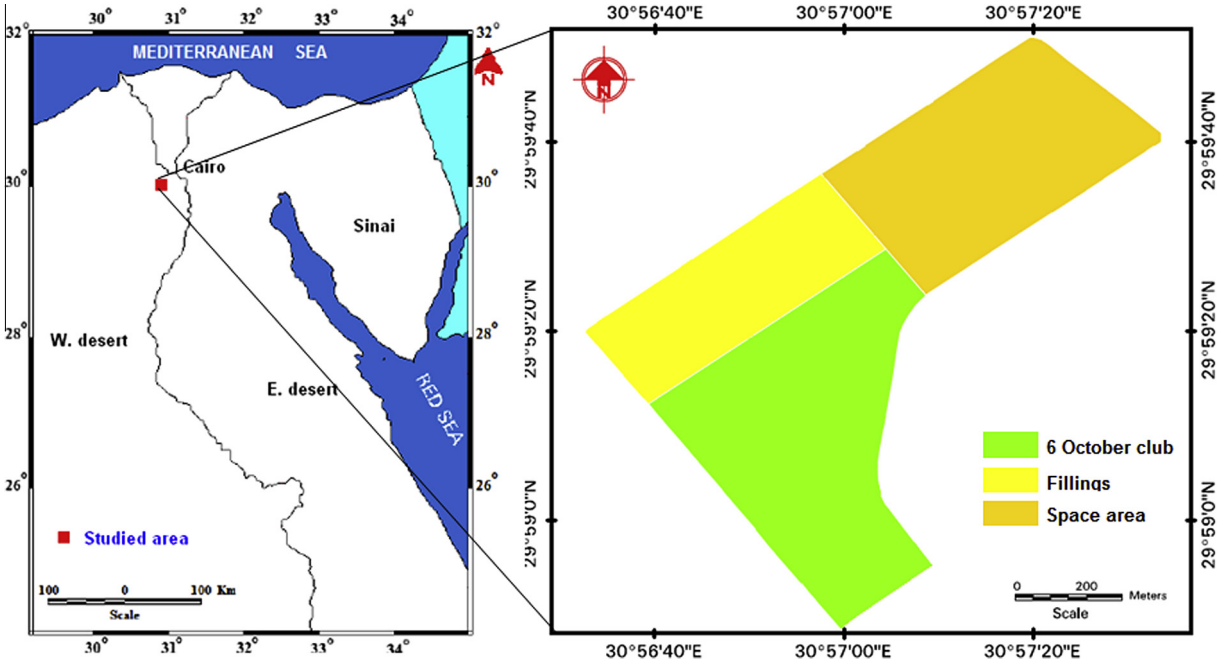

Fig. 1 Location map of the studied area.

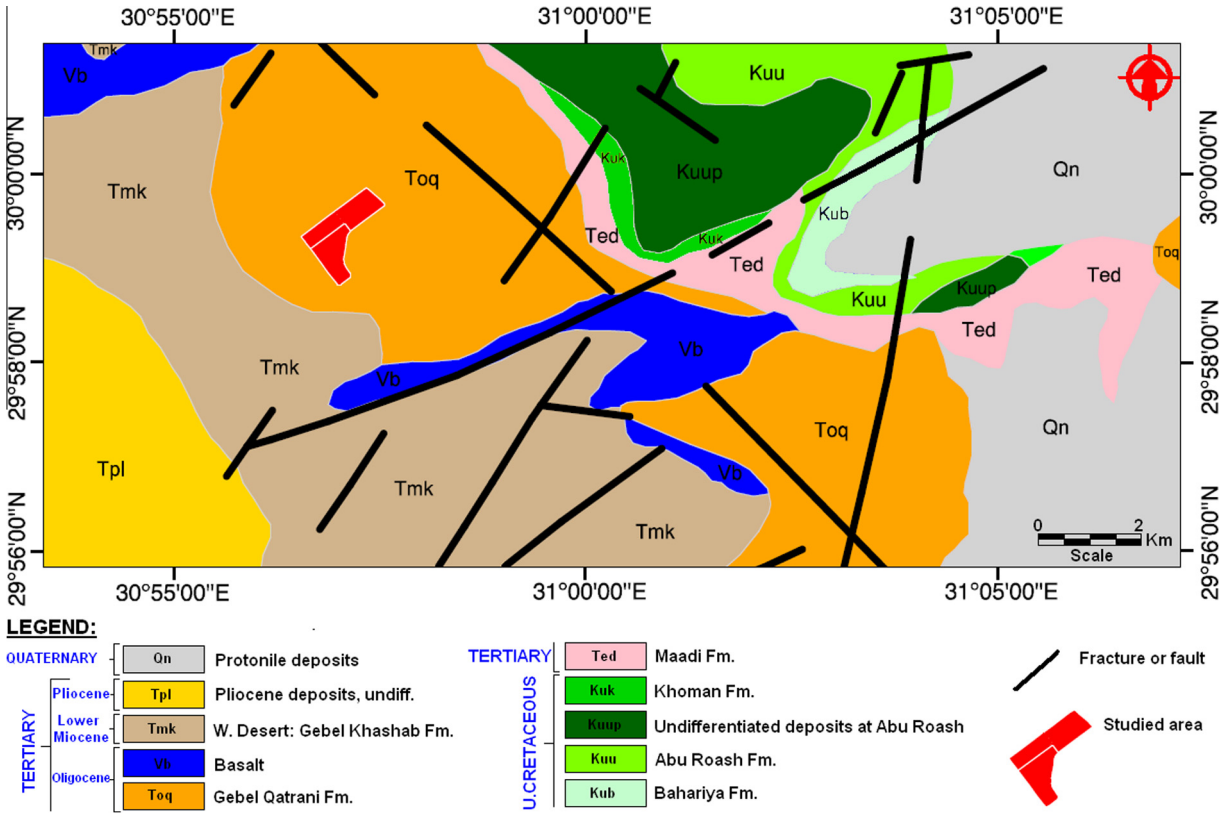

Fig. 2 The Geological map of the interested area (modified after Conco Coral, 1987).

mixture of sand, silt, gravel, clay, and rock fragments, except the top soil layer in some places.

3. Methodology

3.1. HVSR Method

The microtremors are caused by the daily human activities; such as the movements of machinery in factories, motor cars and people walking; and the natural phenomena, such as the flow of water in rivers, rain, wind, variation of atmospheric pressure and the oceanic waves. However, microtremors are now not regarded as nuisance "noises", but rather a useful "signal". In this sense, they are sometimes referred to as "uncontrolled signals". Nakamura (1989) proposed the basis of qualitative arguments that, the Horizontal-to-Vertical Spectral Ratio (HVSR) is a reliable estimation of the site response to the S-wave, providing reliable estimates, not only for the resonance frequency, but also for the corresponding amplification. These ratios are much more stable than the noise spectra and that, on soft soil sites; they exhibit a clear peak, which is well correlated with the fundamental resonance frequency. HVSR data from the ambient noise recordings imply both reliability of the results and rapidity of the data collection.

The interested area, which covers an area of about 1.3 km^2, is classified into grid with cell dimensions of 315 × 240 m (as shown in Fig. 3) where R1 represents the first row (SW–NE) and C1 represents the first column (SE–NW), in the grid. So, each site location is represented by a row number and a column number (e.g. R1C1) and there is an additional site located at the top of hill exposure.

The frequency content of the microtremor record is distributed over a wider range and the measurement of the ambient vibrations through an array of sensors has appeared as a promising option to complement active sources (Asten and

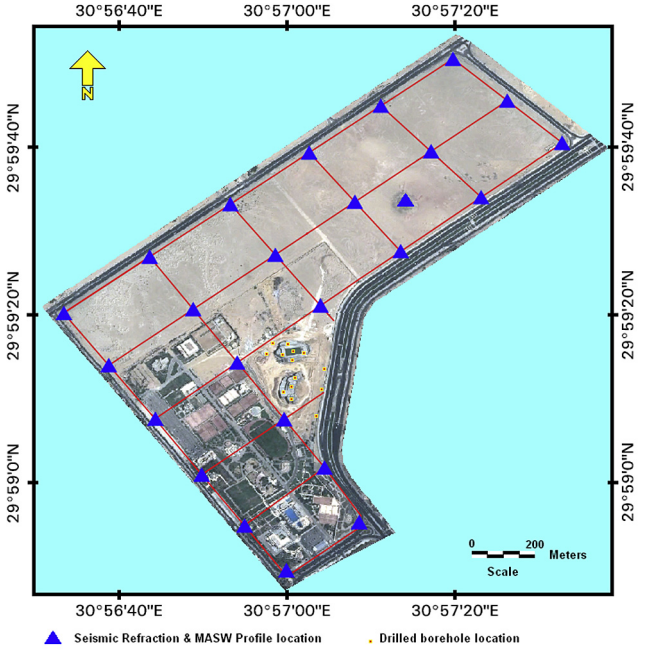

Fig. 3 Classification of the studied area into grid with dimensions 315 × 240 m.

Henstridge, 1984). The noise energy depends upon the source locations and upon the impedance contrast between the rocky basement and the overlying soft sediments (Chouet et al., 1998). The main hypothesis for using the ambient vibration is that, they are dominantly composed of surface waves, which allow the dispersion property to be used (Tokimatsu, 1997).

The microtremor measurements were done at 25 site locations (continuous measurements for at least two hours at each site) at the studied area with the following precautions, according to Duval (1994), Nakamura (1996), Mohamed (2003) and Bard (2007) and SESAME project guidelines:

(1) Carrying out measurements, using 1 s (or higher) tri-axial velocity-meter, for the analysis at periods longer than 1 s.
(2) Avoid long external wiring, which may bring into mechanical and electronic interferences.
(3) Avoid measurements in windy or rainy days. Wind causes large and unstable distortions at low frequencies.
(4) Avoid recordings close to roads with heavy vehicles, which cause strong and rather long transients.

The Taurus Portable Seismograph is used as a data logger, which incorporates a three-channel 24-bit Digitizer, GPS receiver and System Clock, removable data storage, and remote communication options. Taurus is configurable locally, using the color display screen. The used three-component seismometer in the current study is Trillium Compact 120s, that provides the convenience and ease of installation, low noise and high clip level.

MICROTREMOR RECORD SHEET

Date 17 / 05 / 2012
Station N° 01
Station Code R1C1
Location October 6 club
City October 6 City

I- COORDINATES

PLANED COORDINATES			TRUE COORDINATES		
Latitude	Longitude	Altitude	Latitude	Longitude	Altitude
29.98085	30.25018		29.98085	30.25018	

II-GENERAL INFORMATION

Temperature at	Start Time	34°C		End Time	35.9°C		
Wind	Strong		Medium		Weak	√	None
Rain	Strong		Medium		Weak		None √
Noise level	High		Medium	√	Low		None
Building density	Dense		scattered	√	None		Other
Nearby structures	Far		Medium		Near	√	Other
Ground type	Rocky		Firm soil	√	Soft soil		Other
Artificial Ground-Sensor Coupling	No	√	Yes		Type		

Transients	None	Few	Moderate	Many	Distance
Cars				√	40 m
Trucks			√		
Pedestrians					
Other					

III- ACQUISITION PARAMETERS

Samples Per Second 100
Start Time 07:10
End Time 09:18
Rec. Duration 128 min.
Data Logger Taurus Serial Number 2507
Sensor Type Trillium Compact 120s Serial Number

IV- REMARKS

Observer: Adel M.E. Mohamed Signature

Fig. 4 The microtremor work sheet record of site R1C1.

Fig. 4 represents the field work sheet of the site R1C1 and all the recording data are listed in Table 1, while Fig. 5 illustrates a representative example of the recorded data.

The raw data were processed using the J-SESAME software developed within the European project (SESAME, 2004). For each site the microtremor record is corrected for the base-line effect to guarantee the stationary assumption validity. Various numbers of windows, with 25 non-overlapping second (2500 samples) duration, were selected among the quietest part of the recorded signals (for each site, 10 windows at least were used). This is done using the STA/LTA anti-trigger algorithm. This time window is sufficiently long to provide stable results in the studied range of frequency. The time series was tapered with a 10% cosine taper for avoiding leakage and an amplitude spectrum is computed using the Fast Fourier Transform (FFT) for all the three components. A bandwidth coefficient value of 40 is used in the current analyses. The smoothing of the spectra of each component is a mandatory analysis operation. In fact, as shown by several authors (e.g., Bindi et al., 2000; Picozzi et al., 2005), it allows the stabilization of the H/V curves, avoiding the presence of spurious peak, due to the seismic or instrumental or numerical noises. Then, the two horizontal components were merged together using a geometrical mean option, as:

$$H = (|x_f y_f|)^{0.5} \quad (1)$$

Table 1 The recorded microtremor records at the area of interest.

Site		Coordinate (degree)		Instruments		Microtremor	
SN	Code	Latitude	Longitude	Data logger	Sensor (s)	Date	Duration (min)
1	R1C1	29.980444	30.949976	Taurus	T.C. 120	17/5/2012	128
2	R1C2	29.982037	30.952385	Taurus	T.C. 120	17/5/2012	120
3	R2C1	29.981924	30.948599	Taurus	T.C. 120	17/5/2012	130
4	R2C2	29.983839	30.951237	Taurus	T.C. 120	17/5/2012	104
5	R3C1	29.983606	30.947184	Taurus	T.C. 120	17/5/2012	122
6	R3C2	29.985443	30.949909	Taurus	T.C. 120	17/5/2012	143
7	R4C1	29.985455	30.945648	Taurus	T.C. 120	17/5/2012	129
8	R4C2	29.987314	30.948359	Taurus	T.C. 120	17/5/2012	121
9	R4C3	29.989201	30.951111	Taurus	T.C. 120	17/5/2012	121
10	R4C4	29.990997	30.953754	Taurus	T.C. 120	15/5/2012	119
11	R4C5	29.992786	30.956419	Taurus	T.C. 120	15/5/2012	122
12	R4C6	29.994585	30.959097	Taurus	T.C. 120	15/5/2012	122
13	R5C1	29.987234	30.944109	Taurus	T.C. 120	16/5/2012	125
14	R5C2	29.989082	30.946901	Taurus	T.C. 120	16/5/2012	135
15	R5C3	29.990881	30.949614	Taurus	T.C. 120	16/5/2012	130
16	R5C4	29.992636	30.952240	Taurus	T.C. 120	15/5/2012	111
17	R5C5	29.994307	30.954760	Taurus	T.C. 120	15/5/2012	122
18	R5C6	29.995979	30.957283	Taurus	T.C. 120	15/5/2012	124
19	R6C1	29.988955	30.942619	Taurus	T.C. 120	16/5/2012	153
20	R6C2	29.990818	30.945463	Taurus	T.C. 120	16/5/2012	138
21	R6C3	29.992556	30.948126	Taurus	T.C. 120	16/5/2012	126
22	R6C4	29.994263	30.950735	Taurus	T.C. 120	15/5/2012	104
23	R6C5	29.995815	30.953104	Taurus	T.C. 120	16/5/2012	118
24	R6C6	29.997366	30.955482	Taurus	T.C. 120	15/5/2012	120
25	T.P.	29.992590	30.953820	Taurus	T.C. 120	18/5/2012	134

T.C.: Trillium compact 120s.

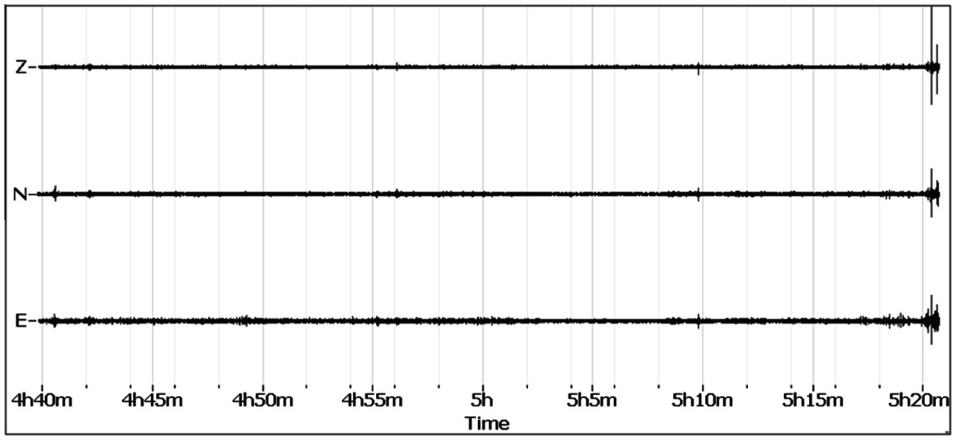

Fig. 5 A sample of the recorded microtremor data of the site R1C1.

where: H is the horizontal component computed by geometrical mean, x_f is the modulus of spectra of the N–S component, and y_f is the modulus of spectra of the E–W component. The horizontal FFT spectra of the 25 s data subsets were divided

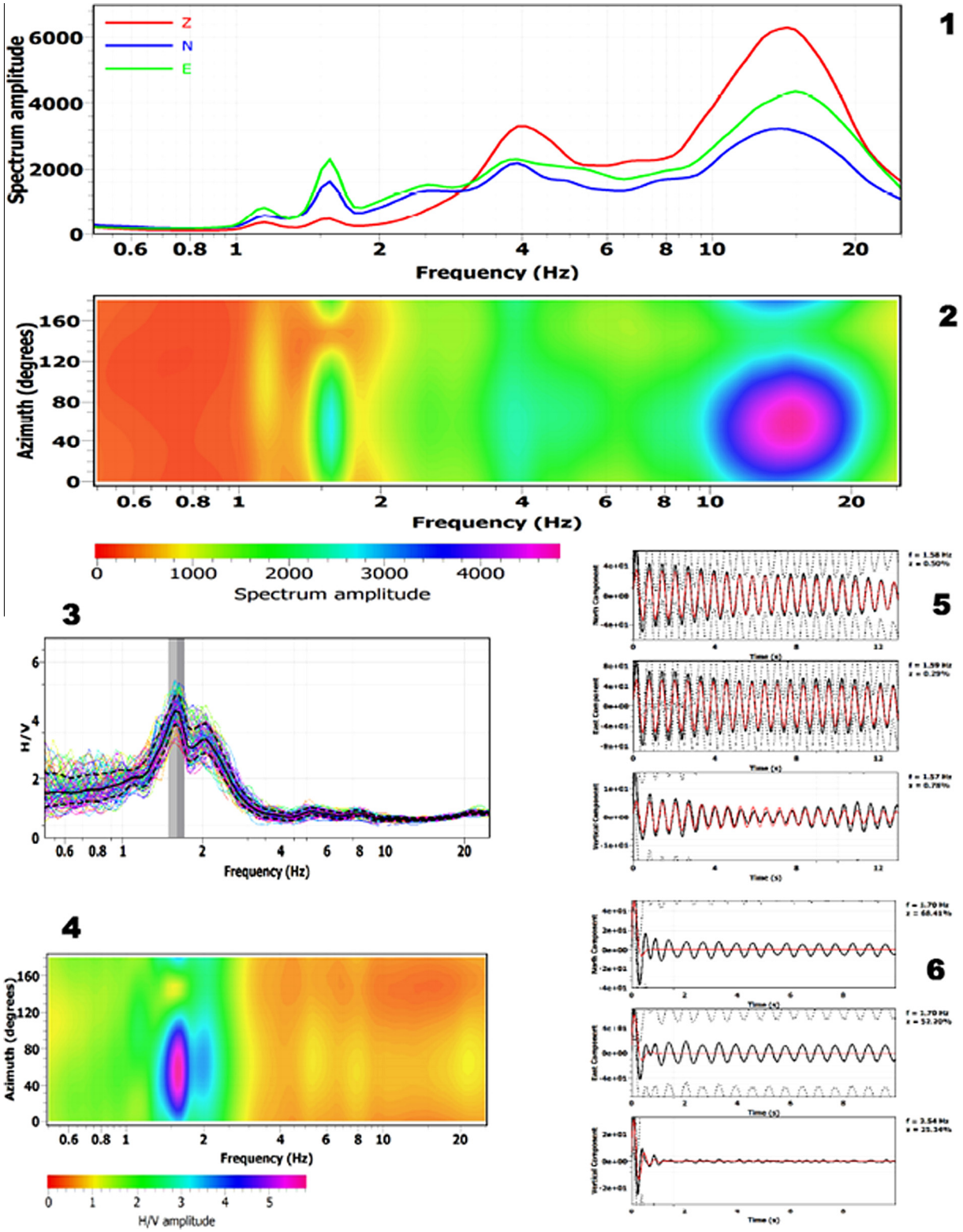

Fig. 6 Panel 1 represents the amplitude spectrum of the three components of the site R1C1, Panel 2 shows the horizontal spectrum rotation with azimuth degrees, Panel 3 demonstrates the H/V spectral ratio curve (amplification at the fundamental frequency), Panel 4 illustrates the H/V rotation with azimuth degrees, and Panels 5 and 6 show the damping test for the peak amplitude at frequency 1.58 Hz which is of industrial origin and at frequency 2.06 which is of natural origin.

by the vertical ones yielding a number of H/V's curves for each site. These H/V's are then averaged and the standard deviations at each frequency of interest are calculated. The resonance frequency and the corresponding amplitude at each site could then be determined. Finally, each peak is checked, if it is of natural or industrial origin, as shown later. Fig. 6 shows an example of such calculation sequence.

The presence of strong sources acting during the recordings may be revealed also by means of a directional analysis of the H/V curves. In order to perform such analysis, the horizontal components of motions are rotated in the 0°-180° degree range and are combined for the H/V computation at regular intervals. This is very useful to check whether a site is 1-D. Like the rotated H/V, J-SESAME computes the spectra with horizontal components spanning different azimuths. The azimuth is regularly counted clockwise from the north. This is useful to check the direction of energy release. The rotated spectra and the rotated H/V curves are conducted for all the sites of interest.

3.2. Broadening of the First-Pulse (Pulse-Width)

The shallow seismic refraction survey was carried out through applying the forward, inline, midpoint and reverse shootings to create the compressional waves (P-waves). Amplitudes of the seismic waves are not only controlled by the geometrical spreading or focusing, but also by the reflection and transmission coefficients, that occur at the discontinuities. Besides this, the wave amplitudes may be reduced, because of the energy loss due to inelastic material behavior or internal friction during the wave propagation. These effects are called intrinsic attenuation. Also, the scattering of energy at small-scale heterogeneities along the travel paths may reduce the amplitudes of seismic waves. In the case of such scattering attenuation, however, the integrated energy in the total wave-field remains constant, while the intrinsic attenuation results in a loss of mechanical wave energy (e.g., by transformation into heat). The wave attenuation is usually expressed in terms of the dimensionless quality factor Q.

Gladwin and Stacey (1974) applied for the P-waves an empirical relation, that relates the pulse duration of the P-waves, the source and the travel path of a seismic wave:

$$\tau_1/2 = \tau_o + (CT/Q_p) \quad (2)$$

where: $\tau_1/2$ is the P-wave pulse duration at a distance d from the source; τ_o is the P-wave pulse duration at the source (at zero distance); C is a constant; T is the P-wave travel time; Q_p is the quality factor for P-wave.

The pulse duration is defined as the linear extrapolation of the maximum slope of the beginning of the pulse before the first onset (using the base-line, as a reference) and the first zero after the maximum of the pulse (Liu et al., 1994). The above mentioned equation is valid for homogeneous media. Wu and Lees (1996) have probed that, this equation can be applied to the fractured media. Jongmans (1991) found that, this method is not valid, when the hypocentral distances are less than 1.2 times the wave length. Gladwin and Stacey (1974) determined the value of the constant c to be equal to 0.5 (for the P-waves).

Applying the pulse-width attenuation relation, the P-wave attenuation for each layer at all sites is determined for the requirement of site effect estimation (Figs. 7 and 8).

The local attenuation (Q_s) for the horizontal shear waves (SH-waves) of the sedimentary column is roughly specified by the following empirical relations of Brocher (2008), due to the absence of such relations for the considered area and the severe lack in records required for achieving such relations:

$$Q_s = -16 + 104.13\ SH - 25.225\ SH^2 + 9.2184\ SH^3 \quad (3)$$

(for: 0.3 km/s < SH (horizontal shear wave velocity) < 5.0 km/s).

$$Q_s = 13 \text{ (for SH} < 0.3 \text{ km/s)} \quad (4)$$

3.3. Site Response

One of the most important and commonly encountered problems in the geotechnical earthquake engineering is the evaluation of ground response. Moreover, it is commonly known that, during earthquakes, the damage to structures is reasonably associated with the underlying subsoil conditions. So, the dynamic properties of the underlying soils are greatly reflected by the characteristics of earthquake ground motions at the ground surface (i.e., ground response). It has also been demonstrated that, the geographic distribution of ground shaking-related damage and its intensity are strongly dependent on the local lithological and physical properties (e.g., silt

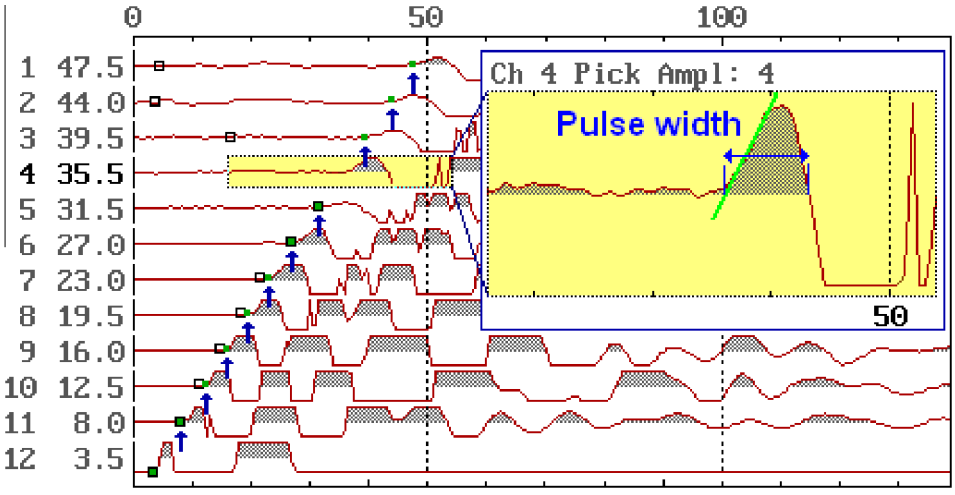

Fig. 7 The Pulse-width for one trace of the seismic profile R1C2.

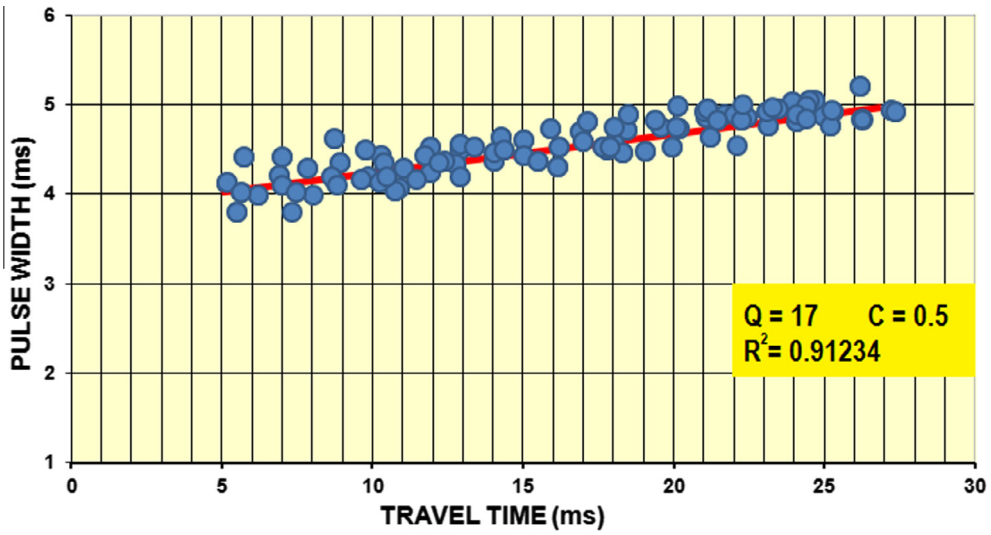

Fig. 8 The attenuation of the second layer as deduced from the relation of the pulse-width and different travel times.

and clay content, as well as void ratio) and conditions (depth-to-water table and basement) of the near-surface sediments (Minakami and Sakuma, 1948; Kanai, 1952; Ooba, 1957; Mueller et al., 1982). This would cause upsurge of groundwater carrying sand, silt and clay in the sedimentary parts of unconsolidated, pours, water-saturated and has a shallow water table (i.e., liquefaction). This is due to the fact that, the stress in such conditions reduces the shear resistance capacity of the soils.

Consequently, understanding the soil effect on the seismic wave became an urgent need, in order to map areas, where amplification is likely and conveying this information to emergency managers and community officials. Moreover, it can be used in land-use planning, reducing business vulnerability, retrofitting building, producing guidelines for new constructions and assisting in infrastructure upgrade. Therefore, over the years, a great effort has been done in the level of theory (e.g., Ohsaki, 1981; Kramer, 1996) and application (e.g., Faeh et al., 1990, 1993, 1994; Zahradnik et al., 1991, 1994; Panza et al., 1996), in order to interpret the earthquake motion characteristics at a site. Both the theory and application are often grouped; according to the dimensionality of the problems they can address (Kramer, 1996).

After addressing the importance of ground response issue, an attempt was made to predict ground surface motions (taking into account the effect of local soil conditions), using the one-dimensional ground response analysis approach. This relies on the theoretical model proposed by Kramer (1996). He stated that, the ground motion at any layer can be easily computed from the ground motion at any other layer (e.g. input motion imposed at the bottom of the soil column), using the *transfer function* ($F_{ij}(w)$), relating the displacement amplitude at layer (i) to that at layer (j), as given by:

$$F_{ij}(\omega) = \frac{|u_i|}{|u_j|} = \frac{A_i(\omega) + B_i(\omega)}{A_j(\omega) + B_j(\omega)} \tag{5}$$

Because of harmonic motion, the acceleration and velocity can be derived from the displacement (i.e., ü = ω ù = ω2 u), Eq. (5) also describes the amplification of acceleration and velocities from layer (i) to layer (j). This equation indicates that, the motion in any layer can be determined from the motion at any other layer. Hence, if the motion at any point in the soil profile is known, the motion at any other point can be contributed and predicted.

4. Results

4.1. HVSR

The results obtained from the microtremor measurements, that were conducted at 25 sites in the study area (which covered by the 6th of October club), using the HVSR technique, demonstrate the fundamental (resonance) frequency (f_o) of the soft sedimentary cover in the study area. There are peaks of industrial origin in the frequency range (1.1–1.65) affecting most of the sites, as shown through Fig. 9 and listed in Table 2. These peaks are attributed to the effect of the main electric power of the wider area.

It is also noted that, the fundamental frequency (f_o) of less than 2 Hz covers the southern part (the area occupied by the gardens and the swimming pool) at the sites R1C2, R2C1, R2C2, R3C1 and R3C2. Values of f_o of less than 2 Hz are located also at the western site (R6C1) and the northeastern part, covering the sites R5C5, R6C5 and R6C6. The low values of f_o (< 2 Hz) at the mentioned sites are attributed to the considerable thickness of the soft sediment section overlying the bedrock. The low values of f_o are compatible with the surface geology, since the studied area is covered by surface sediments of loose to very loose sands, silts, gravels, clays and rock fragment materials.

It is straightforward to identify the following general characteristics of the investigated area, as shown in Fig. 9:

- Most of the area is dominated by low resonant frequency range (1.49–2.68 Hz), which is in consistency with the general geology of the area, indicating that most of the area has a considerable sedimentary section.

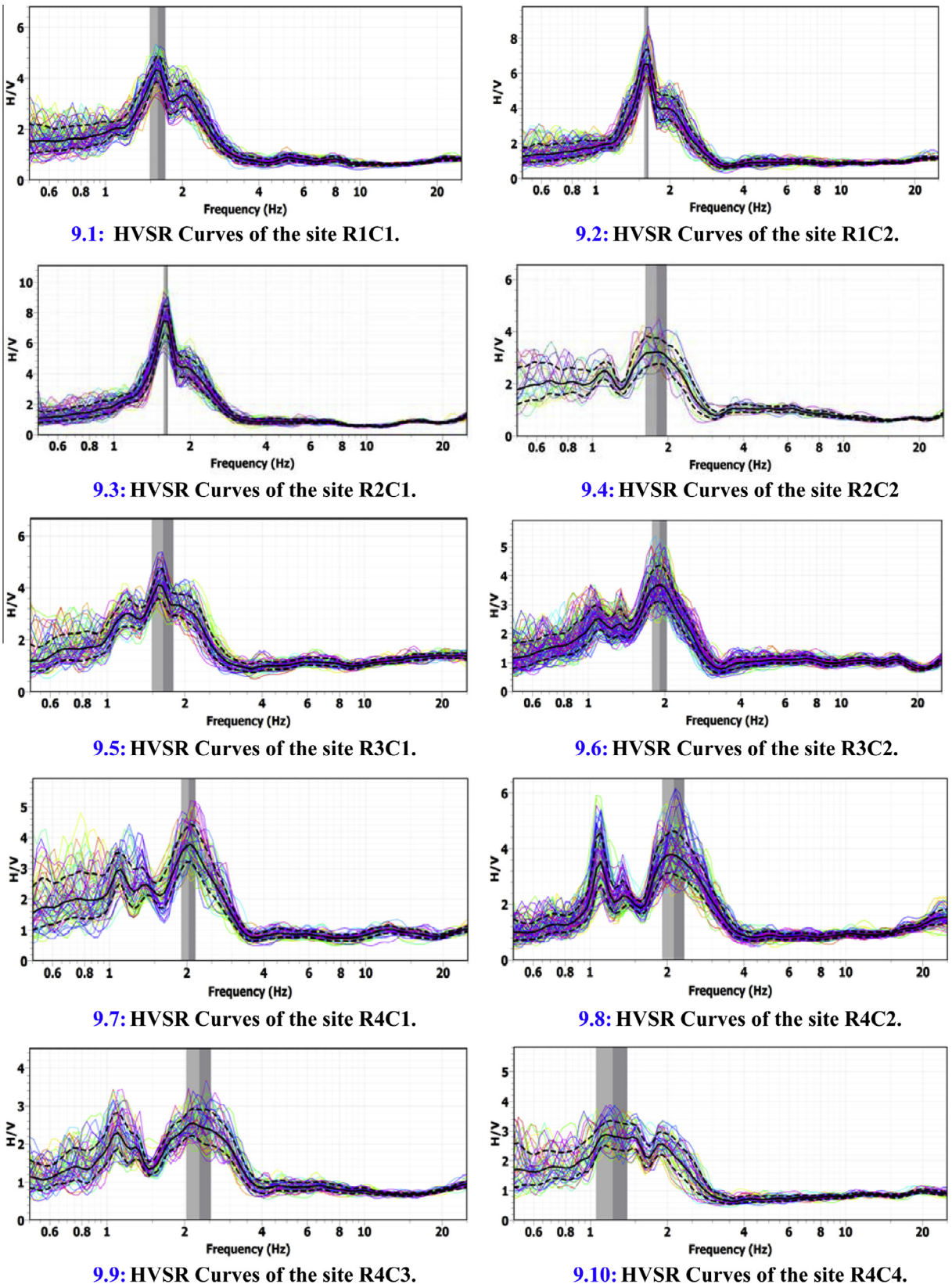

Fig. 9 HVSR curves of the site R1C1, R1C2 R3C1, R3C2, R4C1, R4C2, R4C3, R4C4, R4C5, R4C6, R5C1, R5C2, R5C3, R5C4, R5C5, R5C6, R6C1, R6C2, R6C3, R6C4, R6C5, R6C6.

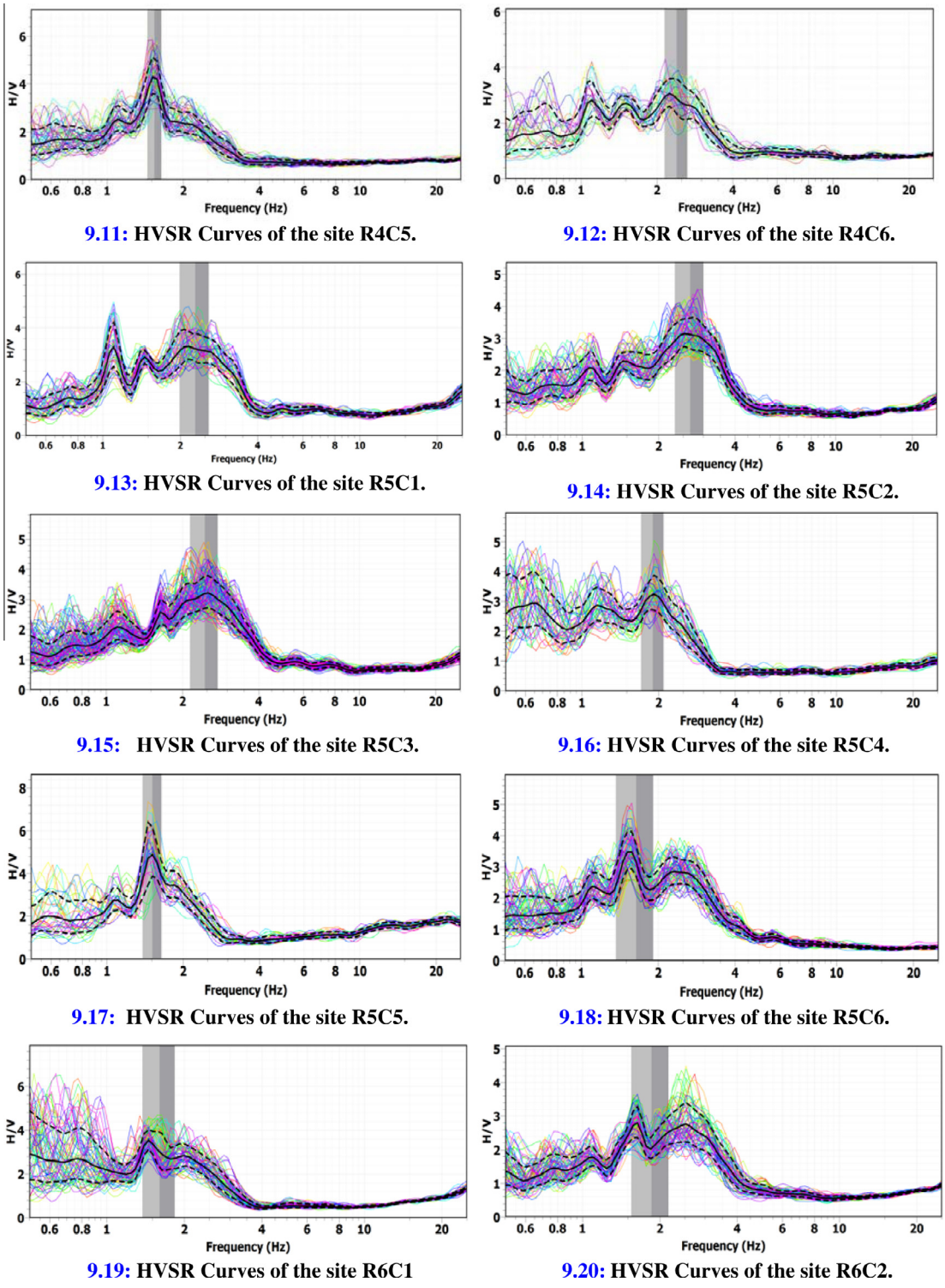

9.11: HVSR Curves of the site R4C5.

9.12: HVSR Curves of the site R4C6.

9.13: HVSR Curves of the site R5C1.

9.14: HVSR Curves of the site R5C2.

9.15: HVSR Curves of the site R5C3.

9.16: HVSR Curves of the site R5C4.

9.17: HVSR Curves of the site R5C5.

9.18: HVSR Curves of the site R5C6.

9.19: HVSR Curves of the site R6C1

9.20: HVSR Curves of the site R6C2.

Fig. 9 (*continued*)

- The low resonant frequency (f_o < 2 Hz) is concentrated mainly at the northeastern, southern and western parts of the investigated area.
- The middle part is characterized by $f_o \geqslant 2$ Hz, which reflects the decreasing of the soft sediment thickness.

4.2. Site Response

A detailed geotechnical model of the October 6 club area was developed using the existing geotechnical data, gathered from the available borehole data and complemented with the

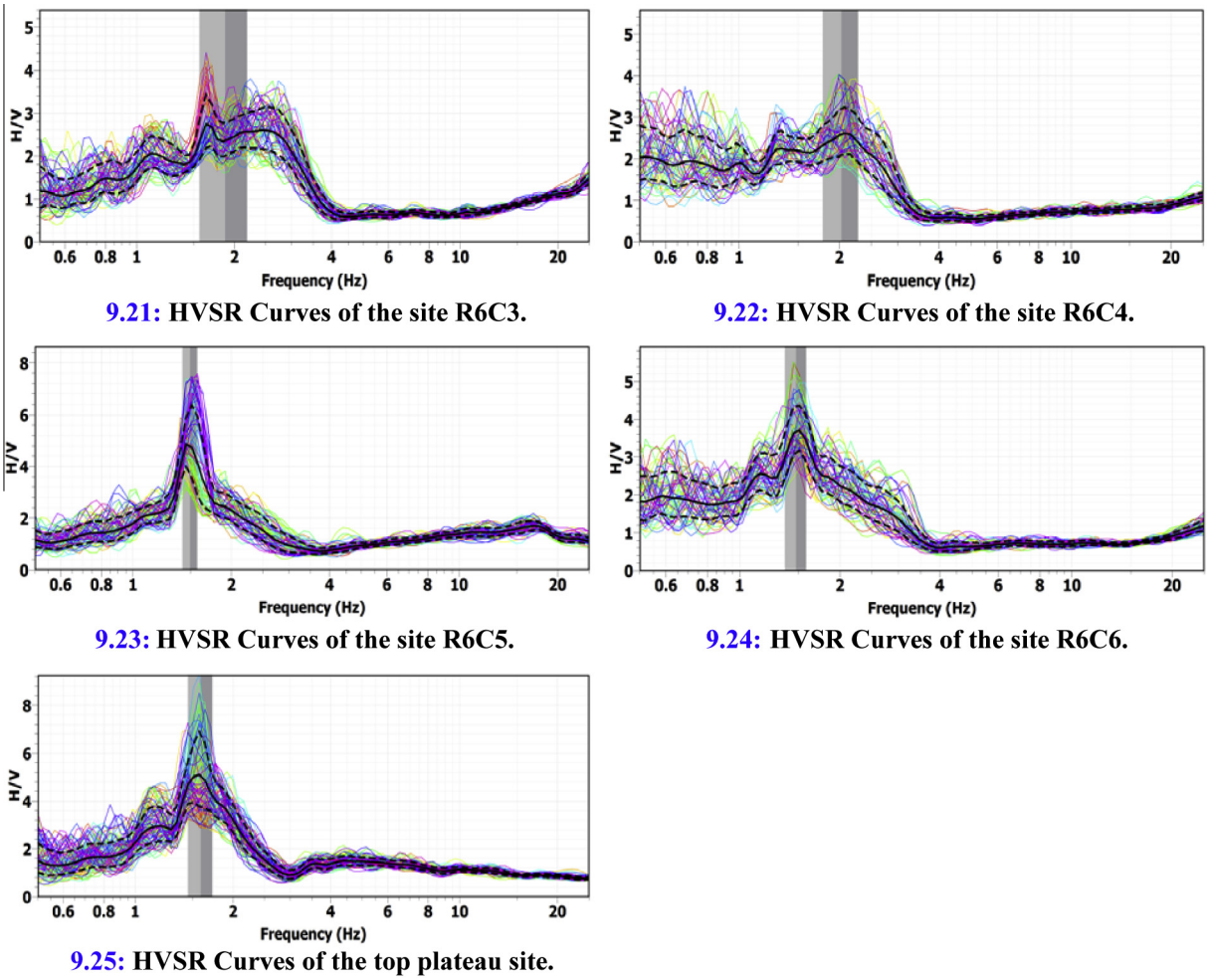

9.21: HVSR Curves of the site R6C3.

9.22: HVSR Curves of the site R6C4.

9.23: HVSR Curves of the site R6C5.

9.24: HVSR Curves of the site R6C6.

9.25: HVSR Curves of the top plateau site.

Fig. 9 (*continued*)

shallow seismic refraction and MASW field work. Mohamed et al. (2013) studied the soil section, in terms of P- and S-wave velocities, using the shallow seismic refraction and MASW techniques. The shear wave velocity is the best indicator of the sediment stiffness (Bullen, 1963; Aki and Richards, 1980), therefore it is recognized, as a key factor for the site response of the soft soil (Borcherdt, 1970).

The amplification of ground motion is proportional to $1/(Vs.\rho)^{0.5}$, where Vs is the shear wave velocity and ρ is the density of the investigated soil (Aki and Richards, 1980). Since the change in density is relatively small with depth, the Vs value can be used to represent the site conditions. Therefore, the shear wave velocities of the soil columns are used in the current study to define the amplification characteristics at the selected 24 sites.

As discussed by Mohamed et al. (2013), the S-wave velocity is derived by inverting the dispersive phase velocity of the surface Rayleigh wave, utilizing the Multi-channel Analysis of Surface Waves (MASW) technique (Park et al., 1999; Miller et al., 1999; Xia et al., 2000). The seismic refraction was carried out through applying the forward, inline, mid-point and reverse acquisition system to create the compressional waves (P-waves). The P-waves are acquired by generating seismic energy using a sledge hammer of 8 kgm, sending the created seismic waves inside the earth. The direct and refracted waves are detected through 40 Hz vertical geophones. The surveyed 24 profiles have 94 m long spread. The geophones, which were firmly coupled to the ground, had 2 m fixed geophone spacing. The technique is to shoot the profile (5 shots) at 5 m distance from both ends, mid-point, in addition to 2 inline shots (between G12-13 and G36-37).

The obtained P- and S-wave velocities and the deduced depth model at the interested area, in addition to the available borehole data, are used to evaluate the ground motion amplification versus frequency.

The results demonstrate the amplification-frequency curves, as shown in Fig. 10 and listed in Table 3, where the (f_o^{30}) is in the range of 3.4 to >20 Hz (down to 30 m depth) and the corresponding ground motion amplification factor is in the range of 1.69–4.74.

The fundamental (resonance) frequency down to 30 m depth (f_o^{30}) distribution map at the interested area (Fig. 11) shows that, the f_o^{30} varies within a short distance, this could be done due to the undulations of the bedrock surface, causing variations in the soil thickness. The soil type also changes from place to place. In the northeastern part of the area, the near-surface bedrock or rocky outcrops are present, while the recent alluvium with variable thickness, with recent or sub-recent clays and silts are present in the southwestern

Table 2 The Fundamental frequency obtained from the HVSR curve.

SITE		Coordinates (degree)		Windows		Frequency		Amplitude		Remarks
SN	Code	Latitude	Longitude	WL(s)	No	F_o	±STD	A_o	±STD	
1	R1C1	29.9804440	30.94997597	40	80	1.58	0.13	4.31	0.55	Industrial
						2.06	0.13	3.32	0.55	Natural
2	R1C2	29.9820366	30.95238495	40	91	1.61	0.02	6.55	0.80	Industrial
						1.94	0.15	4.03	0.73	Matural
3	R2C1	29.9819241	30.94859886	40	86	1.6	0.03	7.44	0.99	Industrial
						1.91	0.15	4.42	0.70	Matural
4	R2C2	29.9838390	30.95123672	40	23	1.12	0.17	2.49	0.36	Industrial
						1.8	0.17	3.24	0.57	Matural
5	R3C1	29.9836063	30.94718361	40	65	1.64	0.14	4.21	0.52	Industrial
						1.9	3.38	3.38	0.43	Natural
6	R3C2	29.9854431	30.94990921	40	119	1.91	0.12	3.66	0.57	Natural
7	R4C1	29.9854546	30.94564819	40	59	2.06	O.l	3.75	0.58	/a:_ira
8	R4C2	29.9873142	30.94835854	40	99	1.1	0.21	3.43		Industrial
						2.12	0.21	3.78	0.89	Matural
9	R4C3	29.9892006	30.95111084	40	56	2.21	0.23	2.52	0.41	/a:_ira
10	R4C4	29.9909973	30.95375443	40	45	1.22	0.16	2.87	0.47	Industrial
						1.9	0.15	2.55	0.41	Matural
11	R4C5	29.9927864	30.95641899	40	57	1.53	0.1	4.21	0.93	Industrial
						2	0.23	2.39	0.47	Matural
12	R4C6	29.9945850	30.95909691	40	31	2.38	0.24	2.98	0.63	/aura
13	R5C1	29.9872341	30.94410896	40	52	2.29	0.28	3.25	0.58	/aura
14	R5C2	29.9890823	30.94690132	40	74	2.68	0.31	3.18	0.46	Matural
15	R5C3	29.9908810	30.94961357	40	128	2.43	0.31	3.22	0.6	/a:_ira
16	R5C4	29.9926357	30.95223999	40	50	1.91	0.16	3.24	0.59	/a:_ira
17	R5C5	29.9943066	30.95475960	40	33	1.5	0.14	4.81	1.51	Industrial
						1.87	0.23	3.42	0.70	Matural
18	R5C6	29.9959793	3O.95728302	40	75	1.55	0.27	3.51	0.61	Industrial
						2.43	0.27	2.84	0.45	Matural
19	R6C1	29.9889545	30.94261932	40	73	1.46	0.22	3.54	0.38	Industrial
						1.98	0.22	2.81	0.56	Matural
20	R6C2	29.9908180	30.94546318	40	78	1.61	0.31	2.78	0.49	Industrial
						2.51	0.31	2.73	0.63	Matural
21	R6C3	29.9925556	30.94812584	40	74	1.65	0.3	2.72	0.67	Industrial
						2.52	0.3	2.6	0.56	Matural
22	R6C4	29.9942527	30.95073509	40	57	2.04	0.22	2.52	0.55	Natural
23	R6C5	29.9958153	30.95310402	40	70	1.49	0.15	4.82	1.48	Natural
24	R6C6	29.9973660	30.95548248	40	64	1.49	0.15	3.59	0.54	Industrial
						1.9	0.21	2.5	0.51	Matural
25	Blatup	29.9973660	30.95548248	40	96	1.56	0.15	5.04	1.24	Industrial
26	East-Blat	29.9973660	30.95548248	40	68	1.51	O.l	5.08	0.91	Industrial
27	West-Blat	29.9973660	30.95548248	40	76	1.49	0.17	4.36	0.79	Industrial
						1.9	0.17	3.3	0.63	Matural
						20.7	0.17	2.79	0.2	Matural

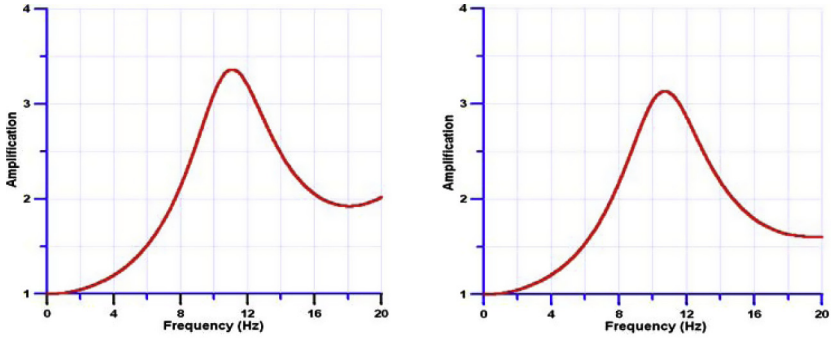

10.1: Amplification curve at the site R1C1.

10.2: Amplification curve at the site R1C2.

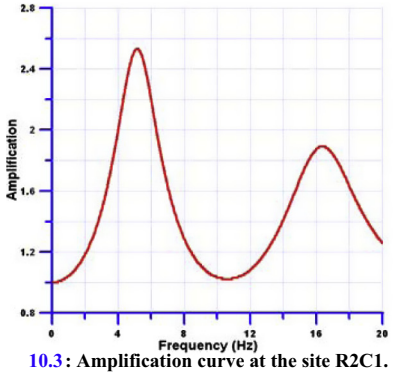

10.3: Amplification curve at the site R2C1.

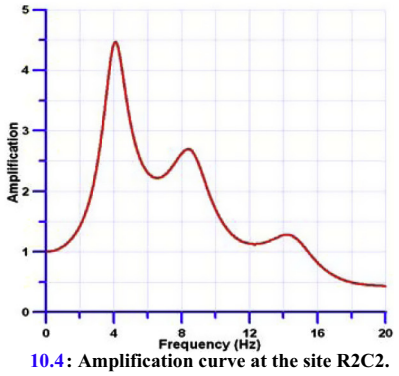

10.4: Amplification curve at the site R2C2.

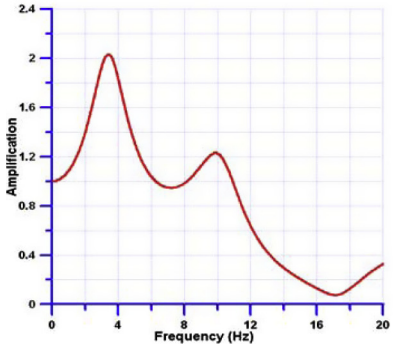

10.5: Amplification curve at the site R3C1.

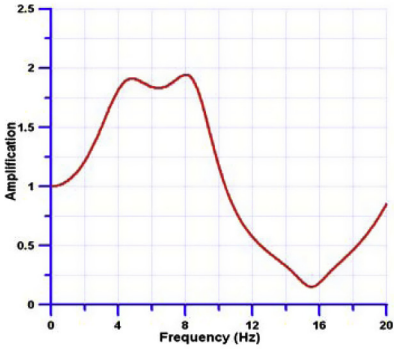

10.6: Amplification curve at the site R3C2.

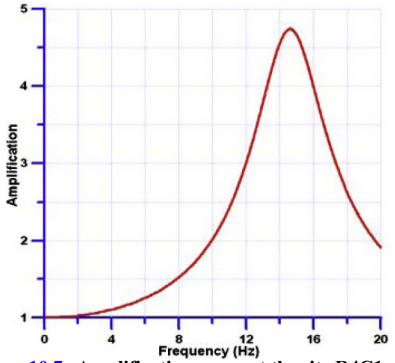

10.7: Amplification curve at the site R4C1.

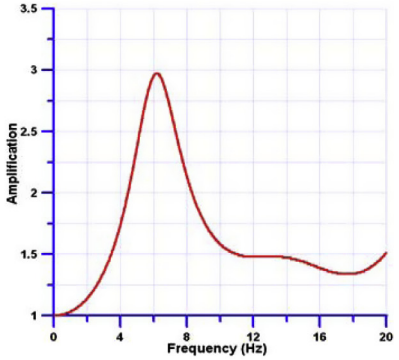

10.8 : Amplification curve at the site R4C2.

Fig. 10 Amplification curve at the site R1C1, R1C2, R2C1, R2C2, R3C1, R3C2, R4C1, R4C2, R4C3, R4C4, R4C5, R4C6, R5C1, R5C2, R5C3, R5C4, R5C5, R5C6. R6C1, R6C2, R6C3, R6C4, R6C5, R6C6.

part. Analyzing the resulting distribution maps of f_o^{30} and the corresponding amplification factor (A_o^{30}) (Figs. 11 and 12), it is straightforward to identify the following general characteristics of the investigated area:

- The f_o^{30} at the northeastern part, which is in consistency with the general geologic features, indicates that the area has a thin sedimentary cover or outcropping bedrock, with higher frequency values (from 12 to >20 Hz).

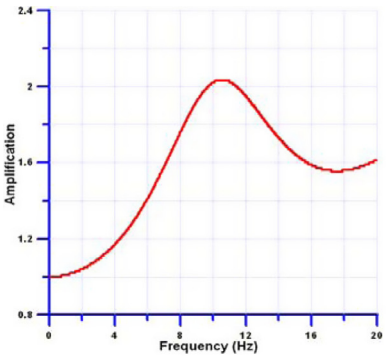

10.9 : Amplification curve at the site R4C3.

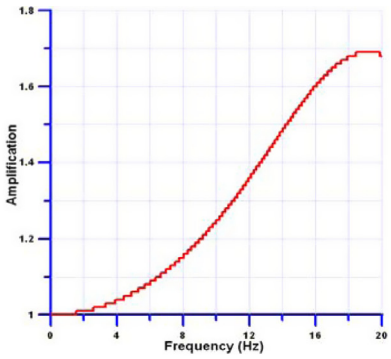

10.10 : Amplification curve at the site R4C4.

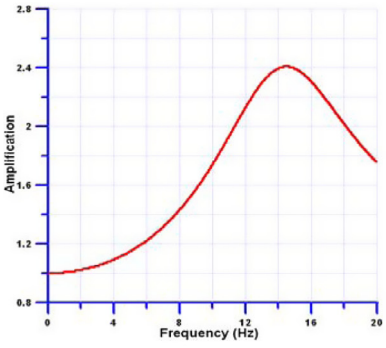

10.11: Amplification curve at the site R4C5.

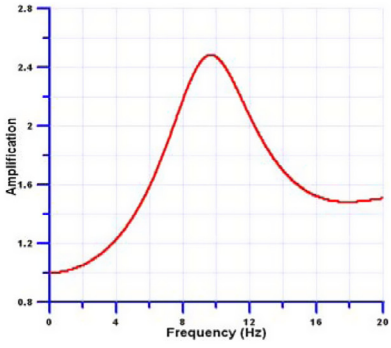

10.12 : Amplification curve at the site R4C6.

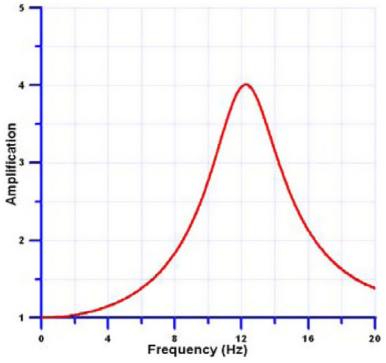

10.13 : Amplification curve at the site R5C1.

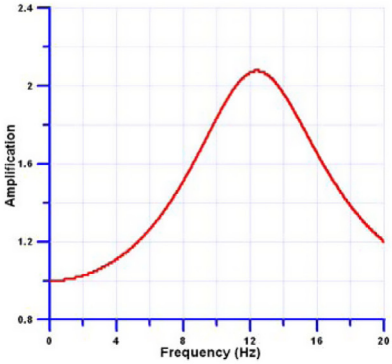

10.14 : Amplification curve at the site R5C2.

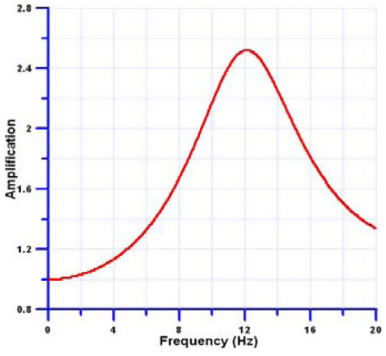

10.15 : Amplification curve at the site R5C3.

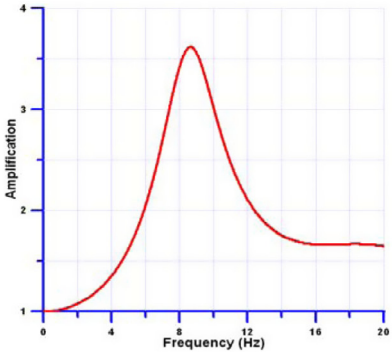

10.16 : Amplification curve at the site R5C4.

Fig. 10 (*continued*)

- The results at the southern part are characterized by lower values of f_o^{30} (from 3.4 to 7 Hz), where the thickness of the soft soil is considerably large.
- The occupied part of low f_o^{30} is characterized by the presence of swelled clay.

The amplification factors are evaluated at the sites of interest at various frequencies; 0.25, 0.5, 1.0, 1.25, 1.5, 2.0, 3.0, 3.0, 5.0 and 10.0 Hz, respectively, as listed in Table 3. The amplification factors at the different frequencies are used for the microzonation. The microzonation, based amplification

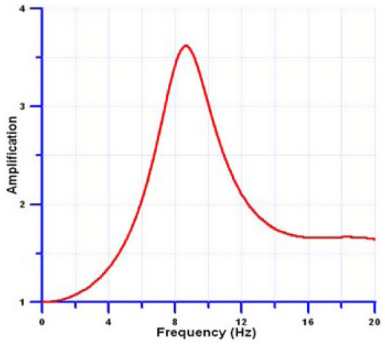

10.17: Amplification curve at the site R5C5.

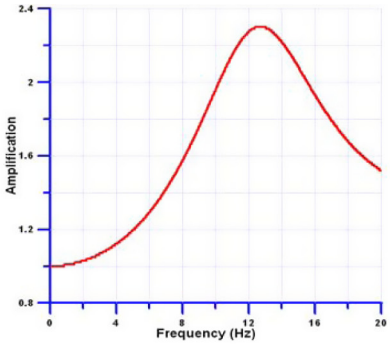

10.18: Amplification curve at the site R5C6.

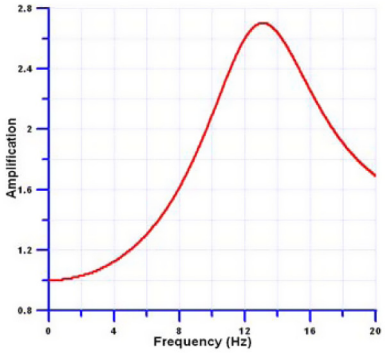

10.19: Amplification curve at the site R6C1.

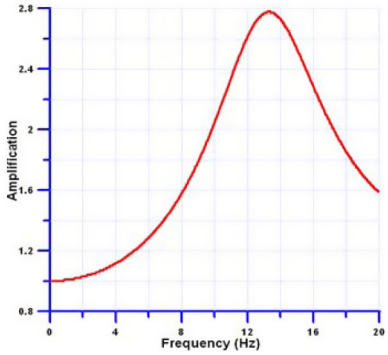

10.20: Amplification curve at the site R6C2.

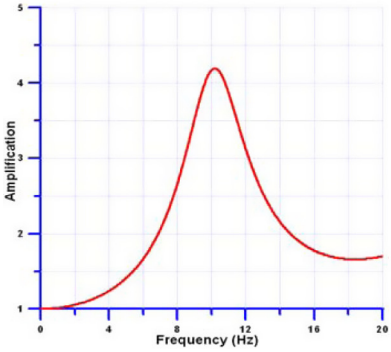

10.21: Amplification curve at the site R6C3.

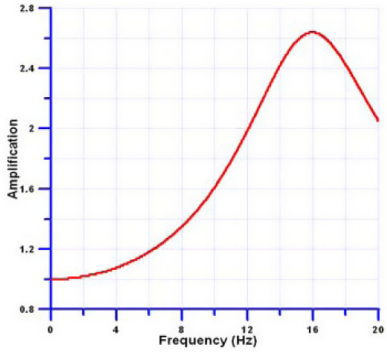

10.22: Amplification curve at the site R6C4.

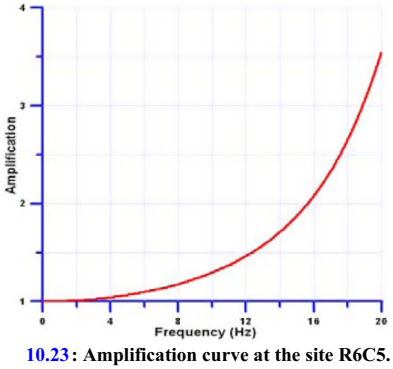

10.23: Amplification curve at the site R6C5.

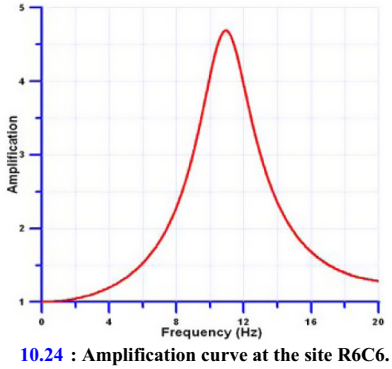

10.24 : Amplification curve at the site R6C6.

Fig. 10 (*continued*)

factor at the investigated sites, demonstrates (Fig. 13): the amplification rating map at frequency 3 Hz (upper left panel), the amplification rating map at frequency 5 Hz (upper right panel), the amplification rating map at frequency 10 Hz (lower left panel) and the amplification rating map at the fundamental frequency (lower right panel).

Table 3 Site effect (amplification at the fundamental frequency and at various frequencies) at 24 sites.

Site		Coordinates (UTM)		VS30		Site response (up to 30 m depth)		Amplification at frequency								
SN	CODE	Easting	Northing	m/s	Class	F. Frequency(Hi)	Amplification	0.25 Hz	0.5 Hz	1.0 Hz	1.25 Hz	1.50 Hz	2.0 Hz	3.0 Hz	5.0 Hz	10.0 Hz
1	R1C1	696828	3151089	318	D	11.1	3.36	1.01	1.01	1.02	1.02	1.03	1.05	1.11	1.33	3.10
2	R1C2	697048	3145636	371	C	10.7	3.13	1.00	1.00	1.01	1.02	1.03	1.05	1.12	1.34	3.04
3	R2C1	695334	3155030	380	C	5.2	2.53	1.00	1.01	1.04	1.07	1.10	1.18	1.47	2.52	1.03
4	R2C2	696967	3155391	400	C	**4.1**	4.47	1.01	1.02	1.09	1.14	1.22	1.43	2.41	3.12	1.70
5	R3C1	695435	3149133	653	C	3.4	2.03	1.00	1.02	1.09	1.14	1.21	1.40	1.94	1.31	1.22
6	R3C2	696407	3149034	379	C	4.8	1.91	1.00	1.01	1.05	1.08	1.12	1.21	1.50	1.91	1.18
7	R4C1	699088	3149156	363	D	14.6	4.74	1.00	1.00	1.01	1.01	1.01	1.03	1.06	1.17	2.02
8	R4C2	694784	3147125	781	B	6.2	2.97	1.00	1.01	1.03	1.05	1.08	1.14	1.36	2.38	1.58
9	R4C3	696523	3147153	405	C	10.5	2.03	1.00	1.00	1.01	1.02	1.02	1.04	1.10	1.30	2.02
10	R4C4	699036	3147116	327	D	19.2	1.69	1.00	1.00	1.00	1.00	1.00	1.00	1.02	1.06	1.24
11	R4C5	694495	3145176	549	C	14.5	2.41	1.00	1.00	1.09	1.09	1.09	1.02	1.05	1.15	1.74
12	R4C6	698970	3145151	463	C	9.7	2.48	1.00	1.00	1.01	1.02	1.03	1.05	1.12	1.38	2.47
13	R5C1	694538	3143056	456	C	12.2	4.01	1.00	1.00	1.01	1.01	1.02	1.03	1.08	1.25	2.78
14	R5C2	696439	3143120	426	C	12.4	2.08	1.00	1.00	1.01	1.01	1.02	1.03	1.06	1.18	1.83
15	R5C3	699090	3142880	289	D	12.1	2.52	1.00	1.00	1.01	1.01	1.02	1.03	1.07	1.22	2.17
16	R5C4	695215	3149976	1262	B	8.6	3.62	1.00	1.00	1.02	1.03	1.04	1.08	1.18	1.62	3.01
17	R5C5	695976	3150089	482	C	8.6	3.62	1.00	1.00	1.02	1.03	1.04	1.08	1.18	1.62	3.02
18	R5C6	697108	3150129	335	D	12.7	2.30	1.00	1.00	1.01	1.01	1.02	1.03	1.06	1.19	1.96
19	R6C1	698074	3150066	390	C	13.1	2.70	1.00	1.00	1.01	1.01	1.02	1.03	1.07	1.20	2.09
20	R6C2	699005	3150176	366	C	13.3	2.78	1.00	1.00	1.01	1.01	1.02	1.03	1.06	1.19	2.04
21	R6C3	695005	3150930	576	C	10.2	4.19	1.00	1.00	1.01	1.02	1.03	1.05	1.13	1.41	4.17
22	R6C4	696326	3151078	388	C	16.0	2.64	1.00	1.00	1.00	1.01	1.01	1.02	1.04	1.12	1.61
23	R6C5	698028	3151031	438	C	> 20	3.54	1.00	1.00	1.00	1.00	1.01	1.01	1.02	1.06	1.29
24	R6C6	698984	3151039	349	C	10.9	4.69	1.00	1.00	1.01	1.02	1.02	1.05	1.11	1.33	4.07

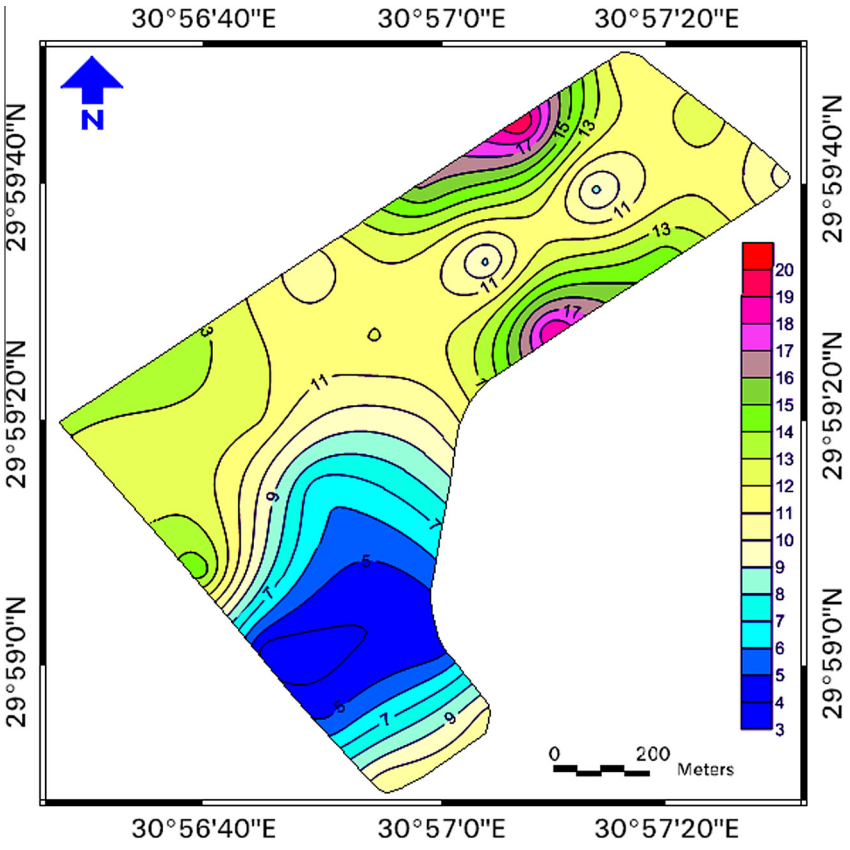

Fig. 11 The fundamental frequency distribution map at the interested area.

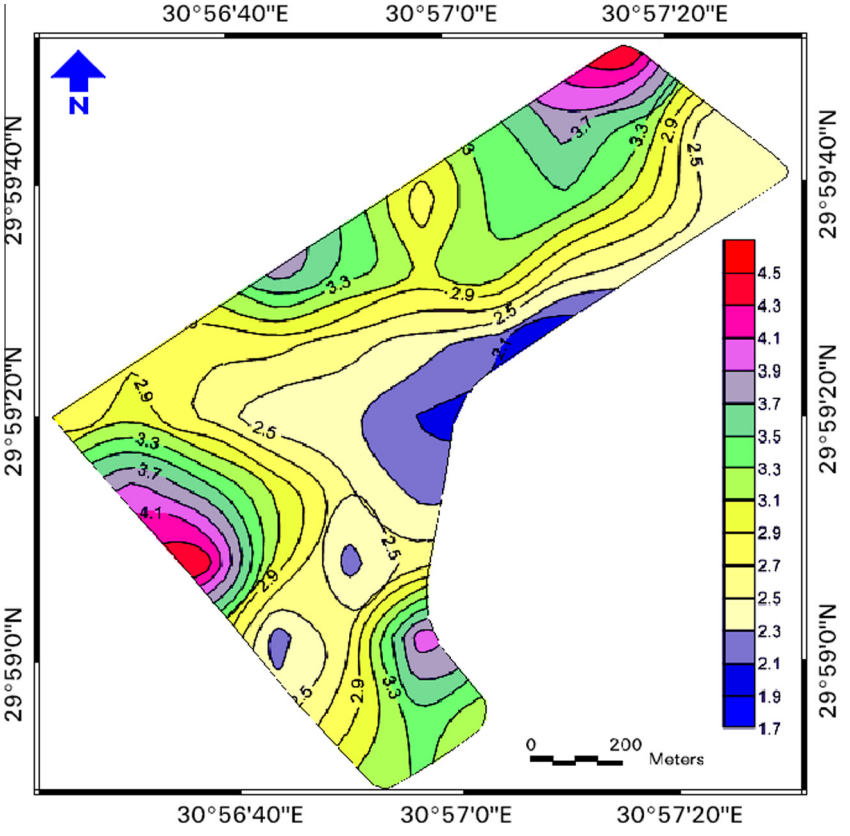

Fig. 12 The amplification at the corresponding fundamental frequency distribution map at the interested area.

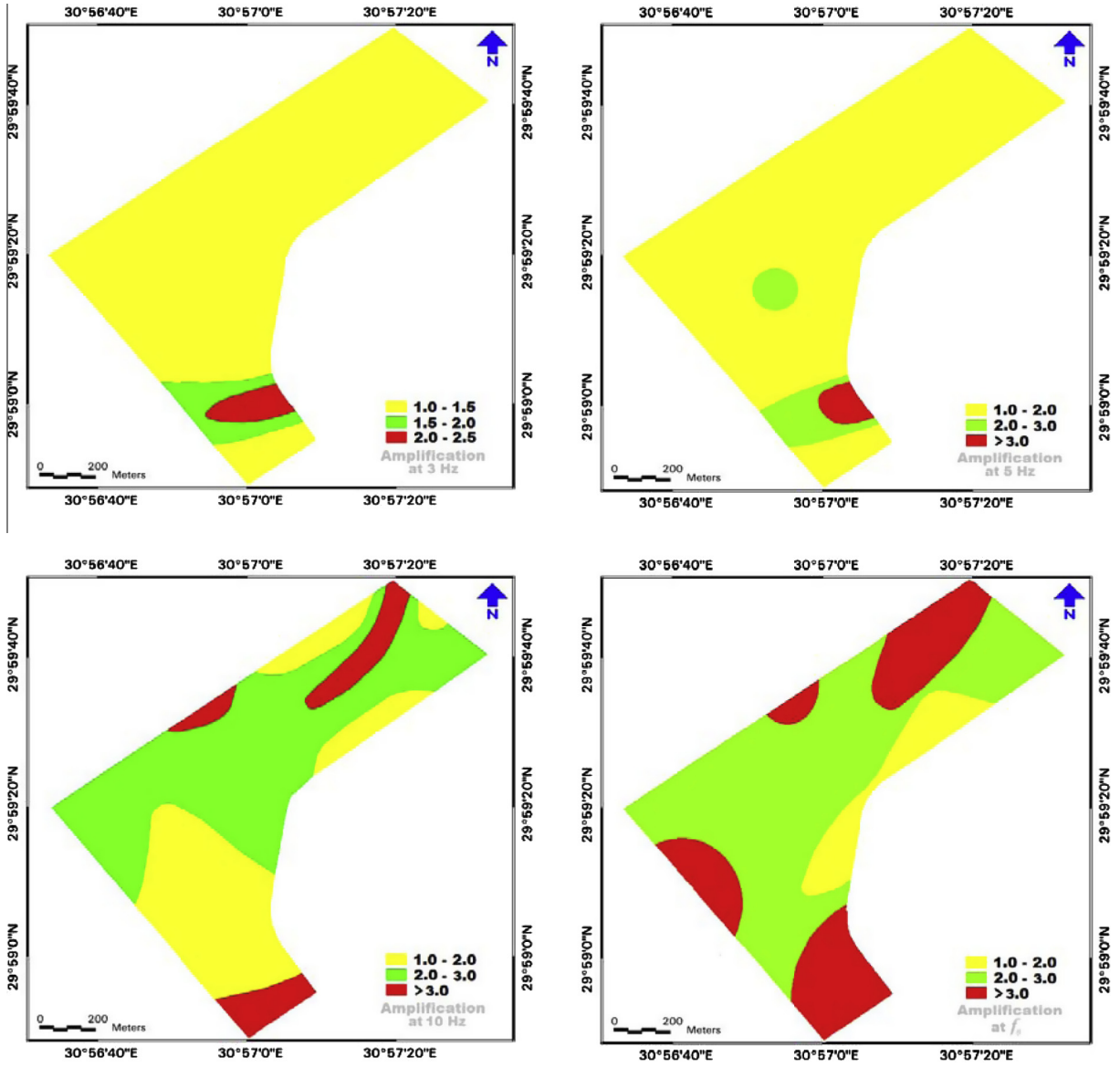

Fig. 13 The microzonation, based amplification factor at the investigated sites, which demonstrates: the amplification rating map at frequency 3 Hz (upper left panel); the amplification rating map at frequency 5 Hz (upper right panel); the amplification rating map at frequency 10 Hz (lower left panel) and the amplification rating map at fundamental frequency (lower right panel).

5. Discussion and Conclusions

Most of the cities and high populated areas (as Cairo City) are located on soft sediments (valleys, estuaries, recent deposits, ...), the soil structures of which are prone to amplify seismic waves. This phenomenon is usually called site effect or site amplification, since the amplitude of the motion highly depends upon the local properties of the soil. Consequently, the risk mitigation requires fine investigations of each geologic setting. The investments necessary with conventional techniques, i.e. boreholes are prohibitive for developing countries and for regions with moderate seismic activities.

The microtremor survey was conducted at 24 sites in the area, which covered the 6th of October club. The results obtained from the HVSR demonstrate the fundamental (resonance) frequency (f_o) of the soft sedimentary cover in the study area. According to the reliability of the HVSR curves, there are peaks of industrial origin in the frequency range (1.1–1.65 Hz) affecting most of the measured sites. These peaks are attributed to the effect of the main electric power. It is also noted that, the fundamental frequencies (f_o) of values less than 2 Hz cover the southern part (the area occupied by the gardens and swimming pool). f_o is less than 2 Hz at the western site (R6C1) and the northeastern part. The low values of f_o (< 2 Hz) at the mentioned sites are attributed to the considerable thickness of the sedimentary cover. The low values of f_o are found to be compatible with the surface geology.

The deduced amplification-frequency curves at the 24 sites of the studied area, demonstrating a fundamental frequency down to 30 m depth (f_o^{30}), are in the range of 3.4 to > 20 Hz. The results reflect that; f_o^{30} at the northeastern part indicates a thin sedimentary cover or outcropping bedrock,

with higher values (12 to >20 Hz). The southern part is characterized by lower values of fundamental frequencies (3.4–7 Hz), where the thickness of the soft soil is relatively large. The low fundamental frequency area is characterized by the presence of swelled clay, and the corresponding ground motion amplification factors are in the range of 1.69–4.74. The amplifications at the various frequencies (0.25, 0.5, 1.0, 1.25, 1.5, 2.0, 3.0, 5.0 and 10.0 Hz) are evaluated.

The microzonations, based amplification factor at frequencies 3, 5, 10 and f_o^{30}, are evaluated, where the zones of amplification are classified into low (1–2), moderate (2–3) and high (>3).

The obtained f_o^{30} values (due to the upper 30 m) are higher than those obtained from the HVSR. This is due to the depth variation, where the f_o values deduced from HVSR are due to a considerable large depth.

References

Aki, K., Richards, P.G., 1980. Quantitative Seismology. Freeman and Co., New York.

Asten, M.W., Henstridge, J.D., 1984. Array estimators and use of microseisms for reconnaissance of sedimentary basins. Geophysics 49, 1828–1837.

Bard, P.Y., 1994. Effects of surface geology on ground motion: recent results and remaining issues. In: Proc. of the 10th European Conf. on Earthquake Engineering, Vienna, pp. 305–323.

Bard, P.Y., 1999. Microtremormeasurements: a tool for site effect estimation? In: Irikura, K., Kudo, K., Okada, H., Sasatani, T. (Eds.), The effects of surface geology on seismic motion. Balkema, Rotterdam, pp. 1251–1279.

Bard, P.Y. 2007. International Training Course on: Seismology, Seismic data Analysis, Hazard assessment and Risk Mitigation (Potsdam, Germany, 7 July–8 September).

Bindi, D., Parolai, S., Spallarossa, D., Cattaneo, M., 2000. Site effects by H/V ratio: comparison of two different procedures. J. Earthquake Eng. 4, 97–113.

Borcherdt, R.D., 1970. Effects of local geology on ground motion near San Francisco Bay. Bull. Seismol. Soc. Am. 60, 29–61.

Brocher, T.M., 2008. Key elements of regional seismic velocity models for long period ground motion simulation. J. Seismolog. 12, 217–221.

Bullen, K.E., 1963. An Introduction to the Theory of Seismology, third ed. Cambridge University press.

Chouet, B., De Luca, G., Milana, G., Dawson, P., Martini, M., Scarpa, R., 1998. Shallow velocity structure of Stromboli Volcano, Italy, derived from small-aperture array measurements of strombolian tremor. Bull. Seismol. Soc. Am. 88, 653–666.

Conco Coral, 1987. The geological map of Egypt with scale 1: 500 000. Dahshour earthquake, Egypt. U.S.G.S., open file report 93-181 Golden Co.

Duval, A.M., 1994. Détermination de la résponse d'un site aux séismes a aide du bruit de fond: Evaluation expérmentale (Thèse de Doctorat). Paris VI, pp. 265 (in French).

Faeh, D., Subhadolc, P., Panza, G.F., 1990. A new method for the realistic estimation of seismic ground motion in megacities: the case of Rome. Earthquake Spectra 9, 643–669.

Faeh, D., Iodice, C., Subhadolc, P., Panza, G.F., 1993. Estimation of strong ground motion in laterally heterogeneous media: model summation-finite differences In: Proceedings of the 9th European Conference of Earthquake Engineering, September 11–16, 1993, Moscow, 4A, pp. 100–109.

Faeh, D., Subhadolc, P., Mueller, St., Panza, G.F., 1994. A hybrid method for the estimation of ground motion in sedimentary basins: Quantitative modeling for Mexico City. Bull. Seismol. Soc. Am. 84, 383–399.

Gladwin, M.T., Stacey, F.D., 1974. Anelastic degradation of acoustic pulse in rocks. Phys. Earth Planet. Inter. 8, 332–336.

Jongmans, D., 1991. Near-source pulse propagation: application to Q-determination. Geophys. Prospect. 39, 943–952.

Kanai, K., 1952. Relation between the nature of surface layer and amplitudes of earthquake motions. Part I-IV. Bull. Earthquake Res. Inst. Tokyo Univ. (I) 30, 31–37.

Kramer, S.L. 1996. Geotechnical earthquake engineering, Published by Pearson Education Ptd. Ltd., Reprinted 2003, Delhi, India.

Liu, H.P., Warrick, R.E., Westerlund, R.E., Kayen, R.E., 1994. In situ measurements of seismic shear-wave absorption in the San Francisco Holocene Bay Mud by the pulse-broadening method. Bull. Seismol. Soc. Am. 84, 62–75.

Minakami, T., Sakuma, S., 1948. The earthquake motions on various formations of the earths' surface observations at Koti City. Tokyo Univ. Earthquakes Res. Inst. Bull. 26, 61–66.

Miller, R.D., Xia, J., Park, C.B., Ivanov, J., 1999. Multichannel analysis of surface waves to map bedrock. Lead. Edge 18, 1392–1396.

Mohamed, A.M.E. 2003. Estimating earthquake ground motions at the northwestern part of the Gulf of Suez, Egypt. (Ph.D. thesis). Fac. Sc., Ain Shams Univ. pp. 93–139.

Mohamed, A.M.E., Deif, A., El-Hadidy, S., Moustafa, S.S.R., El Werr, A., 2008. Definition of soil characteristics and ground response at the northwestern part of the Gulf of Suez, Egypt. J. Geophys. Eng. 5 (2008), 420–437. http://dx.doi.org/10.1088/1742-2132/5/4/006.

Mohamed, A.M.E., 2009. Estimating the near surface amplification factor to minimize earthquake damage: a case study at west Wadi Hagoul area, Gulf of Suez, Egypt. J. Geophys. Prospect. 57, 1073–1089. http://dx.doi.org/10.1111/j.1365-2479.2009.00796.x.

Mohamed, A.M.E., Araffa, S.A.S., Mahmoud, N.I., 2012. Delineation of near-surface structure in the Southern Part of 15th of May City, Cairo, Egypt using geological, geophysical and geotechnical techniques. Pure Appl. Geophys. 169 (2012), 1641–1654. http://dx.doi.org/10.1007/s00024-011-0415-y.

Mohamed, A.M.E, Abu El-Ata, A.S.A, Abdel Azim, F, amd Taha, M.A., 2013. Site-specific shear wave velocity investigation for geotechnical engineering applications using seismic refraction and 2D Multi-channel Analysis of Surface Waves. NRIAG J. Astron. Geophys.http://dx.doi.org/10.1016/j.nrjag.2013.06.012.

Mueller, C.S., Boore, D.M., Porcella, R.L., 1982. Detailed study of site amplification at El Centro strong motion array station No. 6. In: Proceedings of the Third International Earthquake Micro-Zonation Conference, vol. 1 Seattle, Washington, pp. 413–424.

Murphy, J.R., Shah, H.K., 1988. An analysis of the effects of site geology on the characteristics of near-field Rayleigh waves. Bull. Seismol. Soc. Am. 78, 64–82.

Nakamura, Y., 1989. A method for dynamic characteristics estimation of subsurface using microtremor on the ground surface Q. Rep. Railw. Tech. Res. Inst. 30, 25–30.

Nakamura, Y., 1996. Real-time information systems for seismic hazard mitigation UrEDAS, HERAS and PIC Q. Rep. Railw. Tech. Res. Inst. 37, 112–127.

Ohsaki, Y., 1981. On subdivision of layers in response analysis of soil deposit as a discrete system, Research Report 81–03, Dept. of Architecture, Faculty of Eng. Univ. of Tokyo.

Ooba, S., 1957. Study of the relation between subsoil conditions and the distribution of damage percentage of wooden dwelling hoses in the province of Totomi in the case of the Tonankai Earthquake of December, 7th, 1994, Tokyo Univ. Earthquakes Res. Inst. Bull. 36, 201–295.

Panza, G.F., Vaccari, F., Costa, G., Suhadole, P., Fäh, D., 1996. Seismic input modeling for zoning and microzoning. Earthquake Spectra 12, 529–566.

Park, C.B., Miller, R.D., Xia, J., 1999. Multi-channel analysis of surface waves. Geophysics 64, 800–808.

Picozzi, M., Parolai, S., Albarello, D., 2005. Statistical analysis of noise horizontal to vertical spectral ratios (HVSR). Bull. Seismol. Soc. Am. 95. http://dx.doi.org/10.1785/0120040152.

SESAME, 2004. Site effects assessment using ambient excitations European research project. <http://sesamefp5.obs.ujf-grenoble.fr>.

Tokimatsu, K., 1997. Geotechnical site characterization using surface waves. In: Ishihara (Ed.), Proc. 1st Intl. Conf. Earthquake Geotechnical Engineering, vol. 3. Balkema, pp. 1333–1369.

Xia, J., Miller, R.D., Park, C.B., Ivanov. J., 2000. Construction of 2-D vertical shear wave velocity field by the multichannel analysis of surface wave technique. In: Proceedings of the Symposium on the Application of Geophysics to Engineering and Environmental Problems, February 2000, Arlington, pp. 20–24.

Wu, H., Lees, J.M., 1996. Attenuation of Coso geothermal area, California, from waves pulse width. Bull. Seismol. Soc. Am. 86, 1574–1590.

Zahradnik, J., Jech, J., Bartak, V., 1991. Predicting ground motion variations at the Turkey-Flat test site, California. PAGEOPH 137, 63–84.

Zahradnik, J., Moczo, P., Hron, F., 1994. Blind Prediction of the site effects at Ashigara valley, Japan, and its comparison with reality. Nat. Hazards 10, 149–170.